Postcollision interaction in sequential x-ray radiative and Auger decays after atomic inner-shell photoionization

L. Gerchikov, P. Lablanquie, J. Palaudoux, F. Penent, S. Sheinerman

Post-Collision-Interaction in sequential x-ray radiative and Auger decays after atomic inner shell photoionization

L. Gerchikov*

Department of Physics, Peter the Great St. Petersburg Polytechnic University, 195251 St. Petersburg, Russia

P. Lablanquie,† J. Palaudoux, and F. Penent‡

Sorbonne Université, CNRS, Laboratoire de Chimie Physique-Matière et Rayonnement, LCPMR, F-75005 Paris, France

S. Sheinerman§

Department of Physics, St. Petersburg State Marine Technical University, 190121 St. Petersburg, Russia

(Dated: June 7, 2023)

Abstract

A quantum many-body approach to treat the post-collision interaction (PCI) effect in the process of inner-shell atomic photoionization followed by sequential x-ray radiative and electron Auger decays of inner-shell vacancies has been developed. The energy spectra of both the emitted photoelectrons and Auger electrons have been calculated, compared with experimental measurements and its PCI distortion has been analyzed. The energy sharing between three emitted particles, photoelectron, Auger electron and photon, drastically changes the energy distribution of electron emission compared to the case of single Auger decay of inner vacancy. Experimentally, the photoelectron energy distribution has been measured in Argon 1s ionization in coincidences with $L_{2,3} - M_{2,3}M_{2,3}$ Auger electrons and doubly charged ions. Comparison of calculated and experimental spectra confirms the validity of the developed theory. Calculated line shapes of the Auger electrons also fairly reproduce the measured earlier LMM Auger lines in Ar atom.

PACS numbers: 31.15.xg, 32.70.Jz, 32.80.Aa, 32.80.Fb, 32.80.Hd

*Electronic address: lgerchikov@mail.ru

†Electronic address: pascal.lablanquie@upmc.fr

[‡]Electronic address: francis.penent@sorbonne-universite.fr
[§]Electronic address: sergei.sheinerman@gmail.com

I. INTRODUCTION

PCI in processes involving inner shell atomic photoionization has been intensively investigated for several decades (see e.g. reviews [1, 2] and a more recent paper [3] with references therein). The interest for this subject is justified by the necessity of understanding the complicated decay dynamics of deep shell vacancies. PCI results from the Coulomb interaction between the emitted electrons and the receding ion in the two- or few- steps processes which occur through the creation and decay of a quasistationary intermediate states. It had been revealed that PCI influences strongly the energy distribution of the emitted electrons. For the case of inner-shell atomic photoionization, that is a subject of the present investigation, the emitted electrons are the photoelectron and one or few Auger electrons following photon absorption by an inner shell electron.

The PCI effect has been mostly studied in processes where the primary created vacancy decays by means of the single Auger (SA) decay. A number of theoretical models, within classical and quantum mechanical approaches, have been developed to describe the PCI distortion of the line shape of the emitted electrons [4–22]. The results of the calculation or predictions according to these models agree rather well with coincidence and non coincidence measurements. [1, 3, 23].

When the primary created vacancy decays by double Auger (DA) or multiple Auger (MA) emission the theoretical description of the PCI distortion had also been developed within classical and quantum mechanical approaches [24–29]. The measured line shapes and shifts of the photoelectron and Auger electron lines in the DA and MA processes [29–33] also agree quite reasonably with the theoretical predictions.

An alternative way of deep shell vacancy decay is the radiative decay (by x-ray emission). In this case, an electron from an upper shell fills in the deep vacancy and a high energy photon is emitted. This radiative process can be followed by the Auger decay of the upper vacancy and PCI effects also revealed in these "Sequential (x-ray) Radiative and Auger Decays" (SRAD) processes and lead to the distortion of the photoelectrons and Auger electrons spectra. These effects have been observed first in the slow photoelectron spectra by detecting in coincidences the Ar 1s photoelectron with a selected charge state of the receding Ar^{n+} ion [32]. The PCI distortion of the LMM Auger spectra for the same case of the Ar 1s photoionization followed by the SRAD processes has been studied in noncoinci-

dent measurements [33]. Also the PCI distortion of the $L_3 - M_{4,5}M_{4,5}$ Auger line associated with the SRAD process following Kr 1s photoionization was reported for a few values of the excess photon energies above threshold [34]. A more recent investigation of the PCI effects in the Kr $L_2 - M_{4,5}N_{2,3}$ Auger spectra was carried out by noncoincident method in a wider energy region [35]. However no systematic studies of the PCI effects in the photoelectron spectra associated with the SRAD processes following deep shell photoionization in a wide range of photon energies have been yet carried out.

So far, two theoretical models have been proposed for the description of PCI distortion of the emitted electron lines in the SRAD processes. A first approach, Ref.[32], replaces the real two step SRAD process by the well known one step SA decay of inner vacancy with some effective width, Γ_{eff}. Its value is chosen to adjust the decay time of SA decay to the cumulative time of sequential radiative and Auger decays of the SRAD process. Thus, the proposed model simulates the time delay between the photoionization event and the Auger electron emission. That is why the effective width model gives an adequate description for the PCI distortion of the Auger electron line shapes, especially in the case where the Auger decay is the slowest one in the SRAD process. The latter case has been validated by comparison with experimental observations [34, 35] However, when applied to the photoelectron spectra this approach has shown less satisfactory agreement [32].

Another approach, Ref.[34], has been developed by using a modification of the quantum mechanical model of the PCI effects in the case of multiple Auger decay [26]. This model was used to study the PCI distortion of the Auger electron spectra. Its application to the PCI distortion of the $L_3 - M_{4,5}M_{4,5}$ Auger line in Kr has shown a good agreement with both measurements [34] and results of the effective width model [32].

Unlike the effective width model the approach of Ref. [34] treats an inner vacancy decay as a two step process. Nevertheless it has the same weakness as the effective width model since it does not take into account the participation of the emitted photon to the PCI energy exchange. The photoelectron and Auger electron PCI energy shifts are assumed to be opposite and equal in magnitude like in the case of simple SA decay. That is why this approach could not be considered as *ab initio*, as well as the effective width model.

In the present paper, we develop an *ab initio* quantum many-body approach for the SRAD process. The theory developed here allows us to describe the energy spectra of three particles emitted in the SRAD process, the photoelectron, the Auger electron and the photon. The

performed analysis shows that PCI distorts also the energy spectrum of the emitted photons in parallel with the distortion of the energy spectra of emitted electrons. The comparison of the calculated spectra with the experimental photoelectron spectra obtained in the present work and with available experimental data on Auger electron spectra [33] shows a good agreement between the developed theory and experimental observations. We also have revealed and discussed the qualitative differences of PCI distortion of the energy spectra of photoelectrons and Auger electrons emitted in the SRAD and SA decay processes.

The exact knowledge of the energies of the initial and final states of Auger transition makes it possible to record the Auger electrons emitted in the SRAD process even by means on noncoincidence measurements. However, it is no longer the case for the photoelectron emission where different channels of inner-shell vacancy decay contribute simultaneously to the photoelectron spectrum. That is why the photoelectron emission in the SRAD process can be studied only by means of coincidence measurements between the photoelectron, the Auger electron and the ion charge state which allows to select a particular SRAD channel. In the present work, such measurements have been carried out for Ar 1s photoionization. The results of our measurements show an excellent agreement with the prediction of the present theory.

Our paper is organized as follows: in Section II, we give the general quantum formalism of PCI for the SRAD process, its implementation within the semiclassical approximation and discuss the most general features of the SRAD emission spectra; in Section III, we describe the experimental setup used to measure the coincidence photoelectron spectra presented in the paper; in Section IV, we compare experimentally measured photoelectron and Auger electron spectra emitted in the SRAD process with our calculations accounting for the PCI. The atomic system of units, $|e| = m_e = \hbar = 1$, is used throughout the paper.

II. PCI IN SRAD PROCESS

A. General formalism

The example of the SRAD process is shown by the following scheme

$$\gamma_0 + A \to A^{+*}(1s^{-1}) + e_{ph} \to A^{+*}(2p^{-1}) + \gamma_1 + e_{ph} \to A_f^{2+}(3p^{-2}) + \gamma_1 + e_{ph} + e_A\,. \qquad (1)$$

The diagrammatic representation of the process (1) is shown in Fig. 1.

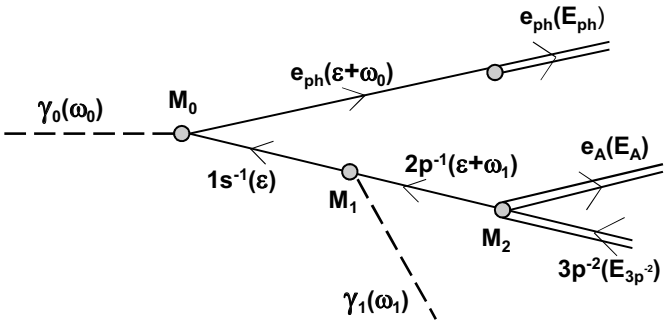

FIG. 1: Diagram of the SRAD process (1)

Here the incident photon γ_0 of energy ω_0 ionizes the $1s$-shell of the target atom A resulting in emission of a photoelectron e_{ph} and creation of a quasistationary $1s^{-1}$ vacancy. In the next step, the $1s^{-1}$ vacancy undergoes radiative decay leading to the creation of a $2p^{-1}$ vacancy and emission of a photon γ_1 of energy ω_1. In the the last step, the quasistationary $2p^{-1}$ vacancy decays with emission of an Auger electron e_A, leaving a residual doubly charged ion A_f^{2+} in its final $3p^{-2}$ state. This Auger decay simultaneously affects the photoelectron motion. We choose this particular SRAD process because it was studied experimentally in Ar and Kr atoms [32–35]. Note that the SRAD process considered here will not limit the generality of the present theoretical section. The theory we develop can be applied to any arbitrary SRAD process as well.

The dashed lines in Fig. 1 represent the incident and emitted photons. The forward solid line represents the photelectron motion in the field of the singly charged ion A^{+*} prior to the Auger decay. The backward solid line represents the quasistationary vacancy states of the singly charged ion A^{+*}. The double forward lines represent the emitted electrons moving in

the field of the doubly charged residual ion A_f^{2+} and the double backward line represents the final double vacancy state of the residual ion. In the parentheses we show the energies of the initial and final states and the virtual energies of the intermediate states. The vertexes of the photoabsorption, photoemission and Auger decay are denoted as M_0, M_1 and M_2, respectively.

The analytical expression for the amplitude of process (1) corresponding to this diagram reads as :

$$A_{SRAD} = \int \frac{d\varepsilon}{2\pi} \frac{\langle e_{ph}(E_{ph})\, e_A(E_A)\, \gamma(\omega_1)\, A_f^{2+} \mid \hat{M}_A\, \hat{M}_1\, \hat{G}(\varepsilon+\omega_0)\, \hat{M}_0 \mid \gamma(\omega_0)\, A\rangle}{\left(\varepsilon - E_{1s} - \frac{i}{2}\Gamma_1\right)\left(\varepsilon + \omega_1 - E_{2p} - \frac{i}{2}\Gamma_2\right)}. \qquad (2)$$

Here $|\gamma(\omega_0)\, A\rangle$ is the vector of the initial state of the atom and incident photon of the energy ω_0; $\hat{M}_0$ is the operator of photoabsorption by an inner–shell electron with the energy E_{1s}; $\hat{M}_1$ is the operator of the radiative decay of $1s^{-1}$ vacancy with emission of photon γ_1 with energy ω_1; $\hat{M}_A$ is the operator of the Auger decay of the $2p^{-1}$ vacancy with simultaneous emission of Auger electron e_A with energy E_A; $\hat{G}$ is the Green function that describes the propagation of the photoelectron in the field of the singly charged ion before its Auger decay; Γ_1 is the decay width of the quasistationary $1s^{-1}$ vacancy state ; Γ_2 is the decay width of the $2p^{-1}$ vacancy state; $|e_{ph}(E_{ph})\, e_A(E_A)\, \gamma(\omega_1)\, A_f^{2+}\rangle$ is the vector of the final state of the doubly charged ion, photon and two emitted electrons: the photoelectron with the energy E_{ph} and Auger electron with energies E_A.

Integration in Eq. (2) along the contour closed in the upper half-plane yields

$$A_{SRAD} = \frac{iM_1M_A}{\omega_1 - E_{2p} + E_{1s} - \frac{i}{2}(\Gamma_2 - \Gamma_1)} \times \qquad (3)$$
$$\left\langle e_{ph}(E_{ph})\, A_f^{2+} \right| \left[\hat{G}\left(\omega_0 + E_{1s} + \frac{i}{2}\Gamma_1\right) - \hat{G}\left(\omega_0 - \omega_1 + E_{2p} + \frac{i}{2}\Gamma_2\right)\right] \hat{M}_0 \left| \gamma(\omega_0)A \right\rangle,$$

The Green function of the photoelectron which propagates from point $\mathbf{r}_1$ to point $\mathbf{r}_2$ can be written as a partial waves expansion:

$$G(\mathbf{r}_1,\, \mathbf{r}_2,\, E) \;=\; \sum_{l,m} \frac{\chi_{El}(r_<)\, \chi^{(+)}_{El}(r_>)}{r_1 r_2} Y_{lm}(\Omega_{r_1}) Y^*_{lm}(\Omega_{r_2})\,. \qquad (4)$$

Here $\chi^{(+)}_{El}$ and χ_{El} are the radial wave functions of the emitted photoelectron moving in the field of singly charged ion, which behave asymptotically as an outgoing and standing wave, respectively; $r_<$, $r_>$ are the lesser and greater of r_1, r_2, respectively.

In the considered SRAD process (1) the photoionization of the 1s atomic shell yields electron with $l = 1$ and we can consider in the amplitude A_{SRAD} (3) the propagation of the p-wave solely. That is why we omit below the index $l = 1$ in the notations of the χ–functions. The amplitude A_{SRAD} is expressed via overlap integrals $\langle\chi|\chi^{+}\rangle$ between the photoelectron wave functions in the intermediate and final states:

$$A_{SRAD} = \frac{iM_0M_1M_A\left(\left\langle\chi_{E_{ph}}\middle|\chi^{(+)}_{\omega_0+E_{1s}+\frac{i}{2}\Gamma_1}\right\rangle - \left\langle\chi_{E_{ph}}\middle|\chi^{(+)}_{\omega_0-\omega_1+E_{2p}+\frac{i}{2}\Gamma_2}\right\rangle\right)}{\omega_1 - E_{2p} + E_{1s} - \frac{i}{2}\left(\Gamma_2 - \Gamma_1\right)} \tag{5}$$

where the factors M_0, M_1, M_A in the Eqs. (3), (5) are the matrix elements of photoabsorption, photoemission and Auger decay, correspondingly. Their product is considered below as a numerical factor which depends slowly on the energies of the emitted electrons. Note that the photoelectron energies in the intermediate states prior the Auger decay are complex. Before the photon emission it equals to

$$E_1 = \omega_0 + E_{1s} + \frac{i}{2}\Gamma_1 = \Delta E + \frac{i}{2}\Gamma_1. \tag{6}$$

Its real part $\Delta E = \omega_0 + E_{1s}$ is the excess photon energy. In the second intermediate state between the $1s^{-1}$ and $2p^{-1}$ vacancies decays the photoelectron energy is equal to :

$$E_2 = \omega_0 - \omega_1 + E_{2p} + \frac{i}{2}\Gamma_2 = \Delta E - \omega_1 + E_{2p} - E_{1s} + \frac{i}{2}\Gamma_2 = Re\{E_1\} - \delta\omega_1 + \frac{i}{2}\Gamma_2. \tag{7}$$

Its real part differs from the excess photon energy $\Delta E = Re\{E_1\}$ by the energy distance of the emission photon energy from its resonance value

$$\delta\omega_1 = \omega_1 - E_{2p} + E_{1s}\,. \tag{8}$$

By introduction of the notation for the overlap integral

$$I\left(E_i, E_{ph}\right) = \langle\chi_{E_{ph}}|\chi^{(+)}_{E_i}\rangle = \int_0^\infty \chi^{(+)}_{E_i}(r)\,\chi^{*}_{E_{ph}}(r)\,dr \tag{9}$$

we rewrite the Eq. (5) as

$$A_{SRAD}(\omega_0, \omega_1, E_{ph}) = \frac{iM_0M_1M_A\left[I\left(E_1, E_{ph}\right) - I\left(E_2, E_{ph}\right)\right]}{\delta\omega_1 - \frac{i}{2}\left(\Gamma_2 - \Gamma_1\right)} \tag{10}$$

It is instructive to consider the limit of very weak PCI, e.g. at high photon excess energies. In this case, the overlap integrals ($i = 1,\, 2$) simply equals to

$$I\left(E_i, E_{ph}\right) = \frac{1}{\left(E_{ph} - E_i\right)} = \frac{1}{\left(\varepsilon_i - \frac{i}{2}\Gamma_i\right)}. \tag{11}$$

Here, we introduce the notation $\varepsilon_{1,2} = E_{ph} - Re\{E_{1,2}\}$ for the energy difference between the final photoelectron energy E_{ph} and the real part of the photoelectron intermediate energy:

$$\varepsilon_1 \, = \, E_{ph} - \Delta E, \quad \varepsilon_2 = E_{ph} - \Delta E + \delta\omega_1. \tag{12}$$

Consequently, the expression (10) for SRAD amplitude reduces to

$$A^{(0)}_{SRAD} = \frac{iM_0M_1M_A}{\left(\varepsilon_1 - \frac{i}{2}\Gamma_1\right)\left(\varepsilon_2 - \frac{i}{2}\Gamma_2\right)}. \tag{13}$$

This simple amplitude corresponds to independent Lorentzian energy distributions of the photoelectrons and the Auger electrons with FWHM Γ_1 and Γ_2, respectively. Indeed, without the PCI energy exchange between emitted electrons a theory should naturally give two independent single particle Lorentzian distributions centered around each single particle resonance energies. For the photoelectron this resonance energy is $\Delta E = \omega_0 + E_{1s} = Re\{E_1\}$. The energy shift from the resonance maximum is $\varepsilon_{ph} \equiv \varepsilon_1 = E_{ph} - \Delta E$. The FWHM of the photoelectron distribution is determined by the imaginary part of its complex energy at the moment of its generation $2Im\{E_1\} = \Gamma_1$.

Similarly the Auger resonance energy is equal to the energy of the Auger transition $2E_{3p} - E_{2p}$. The energy shift from the resonance maximum is $\varepsilon_A = E_A + E_{2p} - 2E_{3p} = -\varepsilon_2$. The last equality follows from the energy conservation

$$E_{ph} + E_A + \omega_1 - 2E_{3p} - \omega_0 = \varepsilon_{ph} + \varepsilon_A + \delta\omega_1 = 0. \tag{14}$$

The FWHM of the Auger energy distribution is naturally equal to the Auger decay width of $2p^{-1}$ vacancy $2Im\{E_2\} = \Gamma_2$.

The exact amplitude $A_{SRAD}(\omega_0, \omega_1, E_{ph})$ of the process (1) has the similar resonance structure as the expression (13) but is distorted by the PCI between two emitted electrons and residual ion. Therefore, the corresponding triple differential cross section $d^3\sigma/dE_{ph}d\omega_1 dE_A$ has resonance pattern. Hence, it is more convenient to write it down via relative energies of the photoelectron, ε_{ph}, Auger electron, ε_A, and emitted photon, $\delta\omega_1$, rather than via their absolute values E_{ph}, E_A, ω_1. Following this line we change the arguments of the SRAD amplitude (10) to $\Delta E, \varepsilon_{ph}, \varepsilon_A$. The triple differential cross section is given by the product of squared modulus of the amplitude (10) and delta function ensuring the energy conservation (14):

$$\frac{d^3\sigma}{d\varepsilon_{ph}d\omega_1 d\varepsilon_A} \propto \mid A_{SRAD}(\Delta E, \varepsilon_{ph}, \varepsilon_A)\mid^2 \delta\left(\varepsilon_{ph} + \varepsilon_A + \delta\omega_1\right). \tag{15}$$

By integration of the triple differential cross section over the emitted photon energies $\delta\omega_1$ we get the double differential cross section for the 2D electron energy spectrum obtained by the coincident measurements

$$\frac{d^2\sigma}{d\varepsilon_{ph}d\varepsilon_A} \propto \mid A_{SRAD}(\Delta E, \varepsilon_{ph}, \varepsilon_A)|^2. \tag{16}$$

According to the Eq.(13) this energy distribution looks like a composition of two Lorentzian energy distributions of the photoelectrons and the Auger electrons with FWHM Γ_1 and Γ_2, respectively, distorted by PCI. In rather common case of $\Gamma_2 \ll \Gamma_1$ the Auger electron energy distribution is much narrow than the photoelectron's one $\varepsilon_A \sim \Gamma_2 \ll \Gamma_1 \sim \varepsilon_{ph}$. Note that the amplitude $A^{(0)}_{SRAD}$ is symmetrical under the exchange between the widths and energies of two emitted electrons: Γ_1 and Γ_2, ε_{ph} and $-\varepsilon_A$. The PCI violates this symmetry, more strongly at the photoionization threshold and slightly at larger excess energies $\Delta E \gg \Gamma_{1,2}$. In particular case of $\varepsilon_{ph} = -\varepsilon_A$ the exact amplitude A_{SRAD} and double differential cross section Eq.(16) are strictly symmetrical under the exchange of the widths.

The single differential cross sections for photoelectron energy spectra measured in non-coincident experiments is obtained by integration of the Eq.(16) over Auger electron energy

$$\frac{d\sigma}{d\varepsilon_{ph}} = \int |A_{SRAD}(\Delta E, \varepsilon_{ph}, \varepsilon_A)|^2 d\varepsilon_A. \tag{17}$$

For the Auger electron spectrum integration over the photoelectron energy should include also the sum over discrete electronic p-states $|\chi_n\rangle$ of a singly charge ion

$$\frac{d\sigma}{d\varepsilon_A} = \int |A_{SRAD}(\Delta E, \varepsilon_{ph}, \varepsilon_A)|^2 d\varepsilon_{ph} + \sum_n |A_{SRAD}(\Delta E, \varepsilon_{ph}, \varepsilon_A)|^2. \tag{18}$$

The sum here corresponds to recapture process contribution to the Auger electron spectrum. Photoelectron relative resonance energy in the case of recapture equals to

$$\varepsilon_{ph} = E_n - \Delta E, \tag{19}$$

where E_n is the energy of the localized electronic p-states $|\chi_n\rangle$ of a singly charge ion.

In the limiting case of $\Gamma_2 \ll \Gamma_1$ the photoelectron energy spectrum has wide Lorentzian profile , while the Auger spectrum is given by PCI distorted Lorentzian profile with the FWHM $\sim \Gamma_2$ In the opposite case $\Gamma_2 \gg \Gamma_1$ the Auger electrons will have wide energy distribution with FWHM $\sim \Gamma_2$ because they originate from Auger decay of the vacancy with large decay width Γ_2. The line width of the photoelectrons emitted from the inner 1s shell will be much narrow, close to 1s vacancy width Γ_1.

B. WKB approximation

The overlap integrals (9) in the SRAD amplitude (10) are the same as in the photoionization amplitude of the SA decay process [21, 29].Such an integral is usually evaluated within the semi-classical approximation of Wentzel, Kramers, Brillouin (WKB). Indeed, the PCI takes place at large distances between the ion and emitted electrons where all Coulomb potentials are smooth and the semi-classical approach can be applied. Hence the wave functions of the intermediate $\chi_{E^{(+)}_{i=1,2}}$ and final $\chi_{E_{ph}}$ photoelectron states in the SRAD process also can be considered in the WKB approximation.

The details of an evaluation of the overlap integrals can be found in the Ref.[21, 29]. Shortly they are reduced to the following. The normalized WKB functions $\chi^{(\pm)}_E$ and χ_E have the form:

$$\chi_E(r) \;=\; \frac{2}{\sqrt{k(r)}}\,\sin\left(\int_{r_0}^{r} k(r)\,dr \;+\; \frac{\pi}{4}\right), \tag{20}$$

$$\chi^{(\pm)}_E(r) \;=\; \frac{1}{\sqrt{k(r)}}\,\exp\left[\pm\, i\left(\int_{r_0}^{r} k(r)\,dr \;+\; \frac{\pi}{4}\right)\right], \tag{21}$$

where r_0 is the radius at which the photoelectron starts out (its value does not influence the line shape); $k(r)$ is the momentum of the electron with energy E moving in the field U of the ionized target and emitted Auger electrons. The evaluation of the overlap integral with these functions is carried out by the saddle-point method. The main contribution to the integral comes from the origin of the the stationary phase point $r = r^*$ where the momenta k_i, and k_f of the intermediate and final photoelectron states coincide. The momenta $k_{i=1,2}(r)$ and $k_f(r)$ are determined from:

$$\frac{1}{2}\,k_i^2(r) \;=\; E_i + \frac{1}{r}; \tag{22}$$

$$\frac{1}{2}\,k_f^2(r) \;=\; E_{ph} + \frac{2}{r} \;-\; \frac{v_1}{v_{12}r}\,, \tag{23}$$

where intermediate photoelectron energies E_i are defined by the Eqs.(6), (7), v_1 and v_{12} denote the photoelectron velocity and the relative velocities between the photoelectron and Auger electrons, respectively. The last term in the r.h.s. of the Eq.(23) comes from the Coulomb repulsion between the emitted electrons.

The saddle point r^* is defined by the conditions $k_i(r^*) = k_f(r^*)$ which leads to the equation

$$r^* \;=\; -\,\frac{C}{\varepsilon_i - i\,\frac{\Gamma_i}{2}}\,, \tag{24}$$

where factor $C = 1 - v_1/v_{12}$. The eventual evaluation of the overlap integral by the saddle point method yields

$$I\left(E_i, E_{ph}\right) = -\frac{i\sqrt{2\pi i C}}{\left(\varepsilon_i - \frac{i}{2}\Gamma_i\right)} \frac{e^{i(\varphi_i(r^*) - \varphi_f(r^*))}}{\left[2E_i - \frac{2}{C}\varepsilon_i + \frac{i}{C}\Gamma_i\right]^{1/4}}. \tag{25}$$

Here the phases $\varphi_{i,f}(r^*) = \int_{r_0}^{r^*} k_{i,f}(r)\, dr$ are equal to:

$$\varphi_{i,f}(r^*) = \left[r \cdot k_{i,f}(r) - \frac{x_{i,f}}{k_{i,f}^{as}} \ln\left(\frac{k_{i,f}(r) - k_{i,f}^{as}}{k_{i,f}(r) + k_{i,f}^{as}}\right)\right]\Bigg|_{r_0}^{r^*}, \tag{26}$$

where $k_{i,f}^{as}$ are the asymptotic electronic momenta at large distances from the atom; $x_{i,f}$ are the effective charges of the mean field potential for given electron state: $x_i = 1$, $x_f = 1 + C$. Below we will use these expressions for the overlap integrals to calculate the SRAD cross sections.

C. Results and discussion

The PCI energy exchange between emitted particles leads to the distortion of their energy spectra, given by the single differential cross sections Eqs. (17), (18). Remind that according to Eq. (13) the energy spectra of the emitted electrons without PCI would be pure Lorentzian.

The PCI manifests both in the line shape distortion and in the energy shift of the spectrum maximum against the peak position of Lorentzian contour without PCI. Experimentally, the latter is determined by the energy spectrum measured at high excess energies where PCI is negligible. We will start the discussion of the differences between the SRAD and the simple single Auger decay processes with this PCI effect.

The PCI energy shift in the case of single Auger decay of inner shell vacancy is very well studied [1–3, 23]. The target ion is too heavy to participate into the PCI energy exchange. Energy is transferred from the photoelectron to the outgoing fast Auger electron due to their Coulomb repulsion. Because of energy conservation $\varepsilon_{ph} = -\varepsilon_A$. Therefore, the same relation is true for the energy positions of the spectra maxima $\varepsilon_{ph}^{\star} = -\varepsilon_A^{\star}$.

In the case of the SRAD photoionization three emitted particles, two electrons and one photon, are involved into the PCI energy exchange. Thus the relation $\varepsilon_{ph} = -\varepsilon_A$ is no

longer valid for the SRAD processes. Instead, according to the Eq.(14), $\varepsilon_{ph} + \varepsilon_A = -\delta\omega_1$. Hence, the relation between peaks positions $\varepsilon^\star_{ph}$ and $\varepsilon^\star_A$ becomes more complicated due to the energy ω_1 of the emitted photon.

There is a simple analytical expression for the PCI energy shift in the case of single Auger decay of the inner shell vacancy [17]

$$\varepsilon^\star_A = -\varepsilon^\star_{ph} = \frac{\Gamma_A}{2v_{ph}}, \tag{27}$$

which is valid if the photoelectron velocity v_{ph} is high enough, $v_{ph} \gg \Gamma_A^{1/3}$, to apply the eikonal approximation and, at same time, is much smaller than the velocity of the Auger electron $v_{ph} \ll v_A$, Γ_A denotes here the width of the inner shell vacancy.

This expression has simple a pure classical interpretation. The negative PCI energy shift of the photoelectron spectrum ε_{ph} equals to the sudden change of ionic potential $-1/r_{ph}$ at the moment of the Auger electron emission, that happens with $2/\Gamma_A = 2\tau_A$ time delay after the inner shell ionization when the photoelectron has moved from the ion by the distance $r_{ph} = 2v_{ph}\tau_A$, $\tau_A = 1/\Gamma_A$ is the Auger decay time. It can be demonstrated that the energy exchange occurring at that distance $r_{ph} = 2v_{ph}/\Gamma_A$ has the largest probability [4].

In the case of the SRAD photoionization a radiative decay of the inner shell vacancy does not change the charge state of the ion. Hence, one can expect that the PCI energy exchange starts at the moment of an Auger electron emission, which occurs with the time delay $\tau_{1s} + \tau_{2p}$ after the $1s^2$ shell ionization, $\tau_{1,2} = 1/\Gamma_{1,2}$ stand here for the lifetimes of the $1s^{-1}$ and $2p^{-1}$ vacancies, respectively. On these grounds, a model for the SRAD process has been proposed in Ref. [32] where its amplitude is given by the WKB amplitude for the single Auger decay with an effective decay width corresponding to the $\tau_{1s} + \tau_{2p}$ lifetime:

$$\Gamma_{eff} = \frac{1}{(\tau_{1s} + \tau_{2p})} = \frac{\Gamma_1 \cdot \Gamma_2}{\Gamma_1 + \Gamma_2}\,. \tag{28}$$

In Fig. 2 we compare the PCI energy shifts of the maxima of the photoelectron spectrum (17), $\varepsilon^\star_{ph}$, and the Auger electron spectrum (18), $\varepsilon^\star_A$, calculated along the line outlined above with predictions $\varepsilon^\star_{eff}$ of the effective width model. All PCI shifts of the spectra maxima have been calculated within the WKB approximation for the photon excess energy $\Delta E =$ 10 eV and the width of the $1s^{-1}$ vacancy $\Gamma_1 = 0.69$ eV as a function of the width of the $2p^{-1}$ vacancy Γ_2. The ratio Γ_2/Γ_1 varies in the plot by two orders of magnitude.

First, note that the behavior of $\varepsilon^\star_{ph}$ and $\varepsilon^\star_A$ reflects the symmetry between the photoelectron and Auger electron spectra under the exchange of the decay widths as it was mentioned

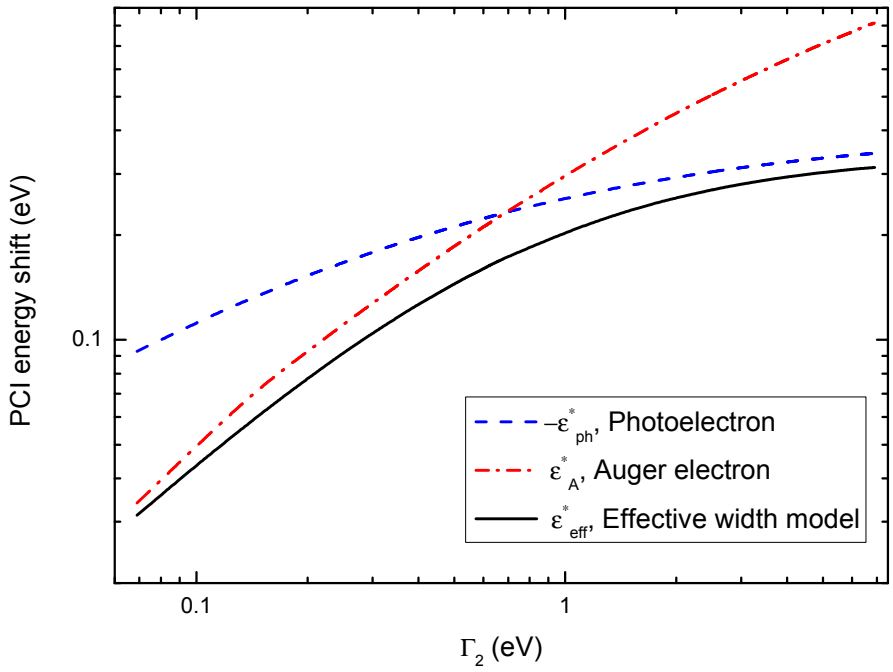

FIG. 2: The PCI energy shift of the photoelectron, $-\varepsilon^{\star}_{ph}$, (blue dashed line) and of the Auger electron, $\varepsilon^{\star}_{A}$, (red dash-dotted line) emitted in the SRAD photoionization processes at photon excess energy $\Delta E = 10$ eV are shown as a function of Γ_2; $\Gamma_1 = 0.69$ eV. The black solid curve shows the PCI energy shift given by the effective width model.

above. Naturally, at the $\Gamma_2 = \Gamma_1$ point the PCI energy shifts coincide, $\varepsilon^{\star}_{A} = -\varepsilon^{\star}_{ph}$. Their absolute values exceed here the prediction of the effective width model by 35%, $\varepsilon^{\star}_{A} \simeq 1.35\varepsilon^{\star}_{eff}$. In the region of the large difference between the decay widths the magnitude of PCI energy shift is governed by the smallest decay width, i.e. by the slowest decay process, in accordance with the effective width model. Moreover, the PCI energy shift of those electrons, which energy distribution FWHM is the smallest of $\Gamma_{1,2}$, approaches $\varepsilon^{\star}_{eff}$. E.g. at $\Gamma_2 = 0.1\Gamma_1$ the Auger electron has the narrowest energy distribution with FWHM $\simeq \Gamma_2$. According to Fig. 2 at this point $\varepsilon^{\star}_{A}$ is very close to $\varepsilon^{\star}_{eff}$, their difference amounts just to 1%. At the same time, the photoelectron has much wider energy distribution with FWHM larger than FWHM of the Auger electron spectrum by one order of magnitude. The smoother energy distribution is more strongly affected by the PCI distortion. That is why $|\varepsilon^{\star}_{ph}| \simeq 3\,|\varepsilon^{\star}_{eff}|$. It means that the emitted photon γ_1 plays an essential role in the PCI energy exchange and

the models neglecting this fact are unable to describe the SRAD process correctly.

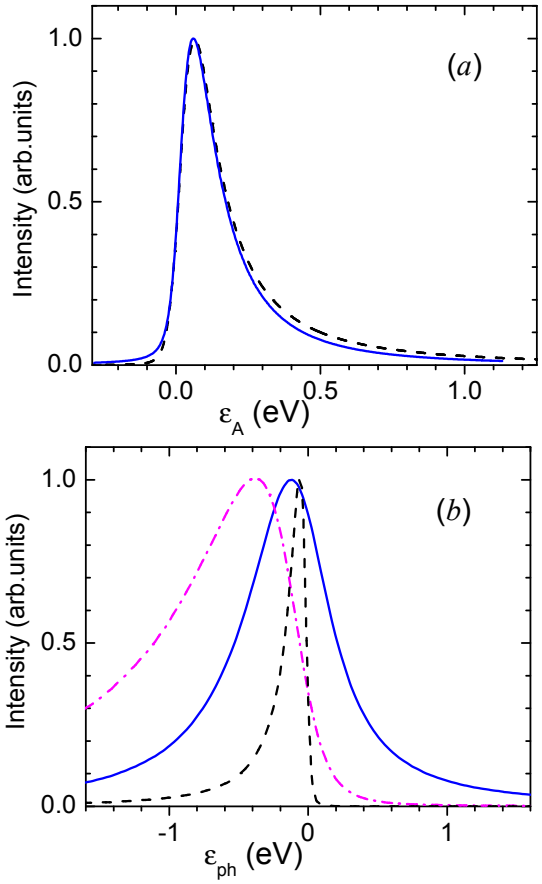

FIG. 3: Energy spectra of 200 eV Auger electrons (see text) (a) and photoelectrons (b) emitted in the SRAD photoionization processes at photon excess energy $\Delta E = 10$ eV calculated with $\Gamma_2 = 0.118$ eV and $\Gamma_1 = 0.69$ eV according to Eqs.(17), (18) are shown by blue solid lines together with results of the effective width model (black dashed line). In addition in lower panel b we show for comparison by dot-dashed magenta line the energy spectrum of the photoelectrons emitted in photoionization process with hypothetical single Auger decay of inner shell vacancy.

In the Fig. 3a,b we compare the line shapes of two electrons emitted in SRAD photoionization process, calculated within the theory developed here, with the predictions of the effective width model and with the emission spectra observed in the hypothetical case of single Auger decay of inner shell vacancy. For this comparison we take the width $\Gamma_1 = 0.69$ eV equal to the width of the $1s^{-1}$ vacancy and $\Gamma_2 = 0.118$ eV equal to the width of the $2p^{-1}$ vacancy of the Ar ion. The effective width (28) in this case amounts to $\Gamma_{eff} \simeq 0.1$ eV. The photon excess energy is taken equal to $\Delta E = 10$ eV and the unshifted Auger electron

resonance energy $E_A = 200$ eV both for the SRAD process and hypothetical SA decay. Here the Auger electron energy is chosen close to the real $L_{2,3} - M_{2,3}M_{2,3}$ Auger decay energies in Ar.

The solid blue curve in the Fig. 3a shows the Auger electron spectrum calculated according to the Eq.(18) within WKB approximation. The black dashed curve shows the Auger electron line shape given by the effective width model with $\Gamma_{eff} = 0.1$ eV. Fig. 3a shows a fairly good agreement between the effective width model and *ab initio* calculations, although we can note a qualitative difference at negative relative energies. Since the spectrum of the effective width model is given by the cross section of SA photoionization process it has sharp cut-off at negative transferred energies, $\varepsilon_A < 0$. On the contrary, the line shape of the SRAD process has more extended left shoulder due to the energy exchange with the emitted photon. The overall good agreement between two approaches is connected with the fact that the Auger decay is the slowest step in this considered SRAD process, Γ_2 is six times smaller than Γ_1. Consequently $\Gamma_{eff} \simeq \Gamma_2$ and the FWHM of Auger electron line is close to the Γ_{eff}. The PCI between two emitted electrons and the residual ion takes place at the distances $r \sim v_{ph}/\Gamma_2 \simeq v_{ph}/\Gamma_{eff}$. Thus the effective width model correctly estimates both the FWHM of Auger electrons energy spectrum and its PCI distortion.

The situation is opposite for the photoelectron spectrum which FWHM $\sim \Gamma_1 \simeq 7\,\Gamma_{eff}$. Fig. 3b shows that the effective width model failed to reproduce the photoelectron line shape. The photoelectron SRAD spectrum shown by blue solid line has been calculated according to the Eq.(17) within the WKB approximation. The black dashed curve shows the photoelectron line shape given by the effective width model. Besides the tremendous difference of the spectrum FWHM the photoelectron PCI energy shift is two times larger than the prediction of the effective width model (see discussion above). It is more interesting to compare the photoelectron SRAD spectrum shown in Fig. 3b by the blue solid line with the hypothetical SA decay photoelectron spectrum with the decay width $\Gamma_A = \Gamma_1$. The latter is shown in Fig. 3b by the magenta dot-dashed line. In spite of comparable FWHM these line shapes are quite different mainly due to large difference of the PCI energy shifts. The PCI energy shift of the magenta curve is determined, according to the Eq. (27), by the width of the 1s shell solely, which we take for this model comparison equal to $\Gamma_A = \Gamma_1 \simeq 6\,\Gamma_2$. This fact explains why the PCI energy shift of the hypothetical SA decay line is three times larger than in the case of the SRAD process. Apart from the large difference of the PCI

energy shifts the SRAD photoelectron spectrum, in contrast with the SA decay case, has more extended right shoulder due to the energy exchange with the emitted photon. This feature makes SRAD photoelectron spectrum more symmetric than the SA decay one. Thus the PCI effects in photoelectron spectra with comparable FWHM are more pronounced in the case of SA decay both in the PCI energy shift and the line shape distortion.

Note once again that the energy spectra of electron emission presented in the Fig.3 and analyzed above correspond to the case of $\Gamma_1 \gg \Gamma_2$. In the opposite case, the picture of the SRAD emission spectra will be similar but with exchange between the photoelectrons and Auger electrons.

It is also worth to emphasize the fundamental difference between energy spectra of SRAD electron emission analyzed above and similar spectra of SA decay. In the case of SA decay the spectral intensity is given by the probability of ionization event resulting in emission of photoelectron and Auger electron which relative energies obey the relation $\varepsilon_{ph} = -\varepsilon_A$. Consequently, photoelectron and Auger electron spectra reflect each other. In the case of SRAD ionization where three particles are emitted the probability of a ionization event is given by the double differential cross section $d^2\sigma/d\varepsilon_{ph}d\varepsilon_A$ (16). Electron spectra presented in the Fig.3 are given by the single differential cross sections $d\sigma/d\varepsilon_{ph}$ (17) and $d\sigma/d\varepsilon_A$ (18). Hence, they do not correspond to one ionization event but give the joint contribution of a set of ionization events where only one particle energy is fixed, e.g. for photoelectron spectrum, $d\sigma/d\varepsilon_{ph}$, we fix the photoelectron energy and integrate in the Eq.(17) over the energy sharing between Auger electron and photon. Therefore, the PCI energy shifts for the photoelectron spectrum maximum, $\varepsilon^\star_{ph}$, and Auger electron spectrum maximum, $\varepsilon^\star_A$, presented in the Fig. 2 correspond to different ionization events. That is why one cannot interpret their sum $-(\varepsilon^\star_{ph} + \varepsilon^\star_A)$ as the photon PCI energy shift because the energy conservation relation (14) is true for the single event of SRAD ionization, i.e. for energy spectrum given by the double differential cross section $d^2\sigma/d\varepsilon_{ph}d\varepsilon_A$. For the same photon excess energy $\Delta E = 10$ eV and the widths $\Gamma_1 = 0.69$ eV, $\Gamma_2 = 0.118$ eV as used in Figs. 2,3 the maximum of the double differential cross section is shifted by the PCI energy distortion by ε_{ph} = -68 meV, $\varepsilon_A = 42$ meV. The corresponding photon PCI energy shift of such energy spectrum equals to $\delta\omega_1 = -\varepsilon_{ph} - \varepsilon_A = 26$ meV. The Eq. (16) for $d^2\sigma/d\varepsilon_{ph}d\varepsilon_A$ allows to analyze the energy sharing between all three emitted particles. We do not present such an analysis here because of lack of experimental data for comparison. The corresponding experimental spectra should

be measured in coincidence experiment with high energy resolution for two emitted particles, two electrons or one electron and photon.

For the same reason, we do not analyze here the photon emission spectrum. To our knowledge no photon-electron coincidence measurements associated with an inner atomic shell photoionization have been reported up to date. So we will restrict ourself here by very brief remarks. It follows from the Eq. (16) that the PCI energy distortion influences the photon spectrum obtained by the double differential cross section and/or measured in the photon-electron coincidence experiments. Of course the photon does not interact directly via Coulomb forces with other charged particles like photoelectron and Auger electron do. The PCI effects originate from Coulomb interaction between the outgoing charged particles. The radiation decay of inner vacancy does not lead itself to the PCI because it does not change the particle charges and PCI starts only on the moment of Auger decay. The PCI effect for the photons is connected with uncertainty of the photon energy due to the finite lifetime of initial, 1s, and final, 2p, states of radiation transition. Within the total photon width $\Gamma_{1s} + \Gamma_{2p}$ the photon energy can vary to suite the most probable condition for the ionization event. The largest probability has the event when two emitted electrons give part of their energy to the photon.

It is also possible to consider the photon spectrum corresponding to the single differential cross section $d\sigma/d\omega_1$. Its evaluation is similar to the Eq.(17), but integrating over ε_A one should keep ω_1 constant and vary $\varepsilon_{ph} = -\varepsilon_A - \delta\omega_1$. Experimentally such spectrum is obtained by photon-electron coincidence measurements where electron are collected in a wide energy range and their energies are not fixed. Our numerical calculations show that PCI effects vanish out completely from the photon single differential cross section: $d\sigma/d\omega_1$ is given by the pure Lorentzian profile with the width equal to the sum $\Gamma_1 + \Gamma_2$ like the case of zero PCI (see Eq.(13)). Thus the photon energy spectrum averaged over all final electron sates is not affected by the PCI. It is quite natural since the photon does not participate directly into PCI via Coulomb forces. But if we fix the energy of one emitted electron we limit the number of final quantum states of the system. It introduces the asymmetry to the photon spectrum simply due to the energy conservation law. In this case emitted photon formally participates to the PCI energy sharing.

III. EXPERIMENT

The experiment was done at the synchrotron SOLEIL on the X-ray beamline GALAXIES [42] . SOLEIL synchrotron was operated in the single bunch mode, providing light pulses every 1184 ns. An asynchronous light chopper [43] was used to extend this light pulse interval to an effective 12 μs The photoionization in the 1s shell of Ar atoms was probed with the HERMES set-up, a magnetic bottle spectrometer of the type initially developed by Eland et al [44]. This apparatus enables to detect in coincidence the 1s photoelectron with the subsequently emitted Auger electrons, through the measurement of their time of flight. A detailed description of the HERMES spectrometer that we used can be found in [45] and reference included. In order to define exactly reaction (1), we collected specifically events where coincidences were recorded between the 1s photoelectron, the Auger electron in the 195-210eV energy range and the residual Ar^{2+} ion. For this purpose the HERMES spectrometer was implemented with an ion time of flight spectrometer. The precise details and performances of this upgraded set-up are given in Ismail et al [46]. Briefly, the magnet assembly defining the electron trajectories in the source region has been designed with an in-axis hole of 4mm diameter, serving as an entrance for the 15cm-long ion time of fight spectrometer. The ion time of flight spectrometer is thus in the axis opposite to the magnetic bottle electron time of flight spectrometer. While a pulsed extraction field was used in [46] to extract the ions, in the present experiment, we used a constant extraction field in the source volume of 3V/cm. This has the advantage to avoid any parasitic signal due to the pulsed field, but slightly reduces the electron resolution, because of the potential drop along the source volume. The source is estimated to be of the order of 300 μm due to the photon beam size, generating a loss in energy resolution of around 100meV while the relative energy resolution $\Delta E/E$ is about 2%. The experimental resolution for the coincidence photoelectron spectra results from the combination of this electron energy resolution with the photon energy resolution, which is around 300meV at 3200eV, in the Ar 1s threshold range. The excess 1s photoelectron energy was defined with respect to the 1s ionization threshold at 3206.26 eV after calibration of the photon energy on the Argon 1s $\rightarrow$ 4p resonance at 3203.54 eV [47].

IV. ELECTRON SPECTRA ASSOCIATED WITH THE SRAD DECAY OF Ar^+ $1s^{-1}$ VACANCY

Here we will apply the developed theory to the electron emission resulting from the ionization of the 1s shell of Argon atom. The $1s^{-1}$ vacancy decay of Ar^+ ion shows a complicated dynamics [32, 36], but its main decay channel leading to the creation of Ar^{2+} ion is the SRAD process presented by the Eq.(1). The radiative decay of the inner vacancy $1s^{-1} \to 2p^{-1} + \gamma_1$ results in the emission of the photon with the energy $\omega_1 \simeq 2960$ eV. The following Auger decay $2p^{-1} \to 3p^{-2} + e_A$ with emission of fast Auger electron e_A ($E_A \simeq 200$ eV) [36] leads to the creation of the Ar^{2+} residual ion. The widths of the 1s and 2p vacancies are equal to $\Gamma_1 = \Gamma_{1s} = 690\,\text{meV}$ [39] and $\Gamma_2 = \Gamma_{2p} = 118\,\text{meV}$ [40].

The photoelectron spectra associated with the SRAD decay channel were obtained by means of coincidences measurements between the 1s photoelectron, the LMM Auger electron and the doubly charged Ar^{2+} ion as it has been explained in the section III. Carrying out such measurements for each photoelectron energy E_{ph} we have collected the Auger electrons in the range 195 - 210 eV that selects all Auger electrons resulting from the $2p^{-1} \to 3p^{-2} + e_A$ Auger transition [33, 37] (the strongest Auger electron line $L_3 - M_{2,3}M_{2,3}$ ($^1D_2$) is centered at 203.47 eV [38]). In the Figure 4 we have presented the measured photoelectron line shapes for the excess photon energies ΔE above the threshold of 1, 2, 4 and 10 eV. These experimental spectra correspond to the photoelectron energy distributions given by the single differential cross section (17). The photoelectron energy profiles calculated according to the Eqs. (17), (10), (25) are shown in the Figure 4 by black solid curves. We chose the integration range in the Eq.(17) 195 eV $< E_A <$ 210 eV according to the experimental conditions. Finally, in order to reproduce the experimental spectra the calculated line shapes were convoluted with a Gaussian profile that takes into account the total experimental resolution function of the electron analyzer. The widths (FWHM) of Gaussian were chosen as FWHM = 300 meV in accordance with the experimental conditions.

Fig. 4 shows a fairly good agreement between the measured and calculated line shapes. Vertical green lines in Fig. 4 show the unshifted photoelectron resonance energies $E_{ph} = \Delta E$. Both the measured spectra and the calculated line shapes exhibit the PCI shifts of the line maximum against ΔE = 0.26, 0.21, 0.17, 0.10 eV for corresponding excess energies $\Delta E = 1, 2, 4, 10$ eV. The widths of the PCI distorted line shapes are varying in the limits

from 0.9 eV to 1.05 eV for the measured curves and from 0.84 eV to 0.93 eV for the calculated curves. These widths are determined both by the widths of vacancies Γ_{1s}, Γ_{2p} and by the FWHM of the experimental resolution function of the electron analyzer, but the main contribution comes from the width of the 1s vacancy $\Gamma_{1s} = 690\,\mathrm{meV}$. Note that the observed SRAD photoelectron spectrum is more symmetric than the photoelectron spectrum associated with the single Auger decay process. This effect is explained by the fact that the SRAD photoelectron spectrum is additionally affected by the energy exchange with emitted photon that leads to more extended right shoulder of the line in contrast with single Auger decay case (see discussion in the section IIC).

Earlier the Ar 1s photoelectron spectra were also measured in coincidence with the doubly charged receded ion, Ar^{2+}, [32], but the Auger electrons were not registered. Since the SRAD process is the main channel of the 1s vacancy decay leading to the final Ar^{2+} ion [36], the measured photoelectron spectra was attributed in the Ref. [32] to process (1). The comparison of the experimental spectra with the predictions of the effective width model revealed its failure in the descriptions of photoelectron spectra.

Concerning the Auger electron spectra, the experimental technique employed in the present paper registers the Auger electrons in coincidence with the photoelectron but does not allow to resolve their energy distribution. The energy spectra of Auger electrons emitted in the same SRAD process (1) have been measured the Ref.[33] where they have been reported at few eV excess photon energies above the Ar 1s threshold.

In the Fig. 5 we show $L_3 - M_{2,3}M_{2,3}(^1D_2)$ Auger electron spectra [33] together with the calculated Auger electron line shapes at the excess photon energy $\Delta E = 2$, 3 eV. We do not consider here smaller excess energies because, near the photoabsorption threshold, the contribution of electron recapture process becomes prominent. Its accurate accounting would require separate considerations which are beyond the framework of the present paper. The theoretical line shapes presented in the Fig. 5 have been calculated as Auger electron single differential cross section (18) with the help of the Eqs. (10),(25). Finally the calculated spectra were convoluted with the Gaussian of FWHM = 180 meV [33] in order to take into account the resolution of the electron detector.

Fig.5 shows a rather good agreement between the calculated and the measured Auger electron spectra. For better visual comparison of line shapes, the calculated curves in Fig. 5 have been shifted by 30 meV to match the energy positions of the experimental peaks.

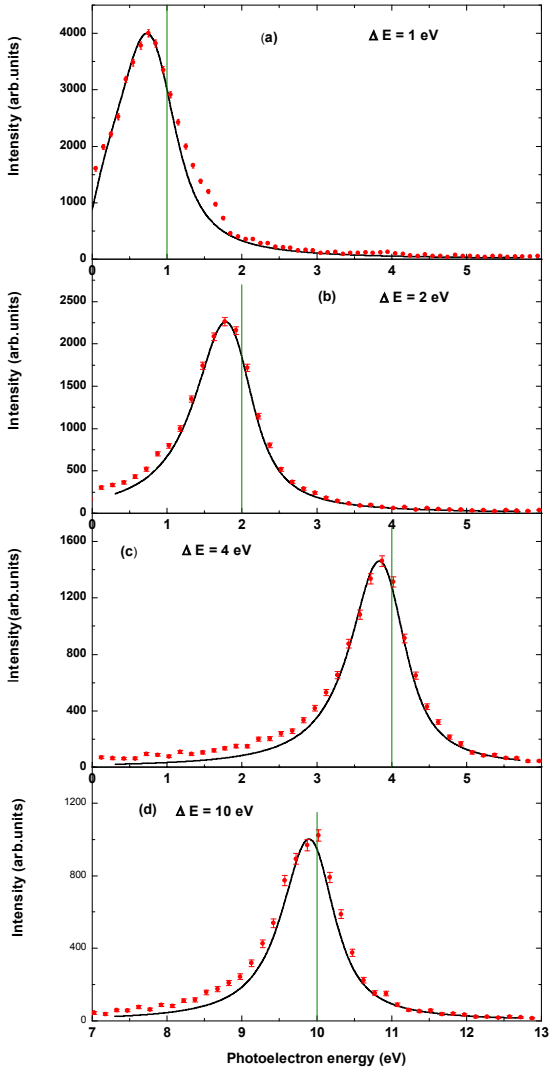

FIG. 4: Photoelectron energy spectra in Ar 1s photoionization followed by SRAD process for the excess photon energies 1, 2, 4, 10 eV (panels (a), (b), (c), (d), correspondingly). Red circles present the measured values whereas the solid black lines show the calculated curves.

This discrepancies between positions of the measured and calculated lines can be attributed to some uncertainties in the experimental calibration of the energy scale. Note that similar disagreement was observed earlier in Ar 1s photoionization followed by SA decay [3].

There is also a small disagreement between the measured and calculated line shapes

at the left profile wing in the energy region below $E_A < 203.37$ eV ($\varepsilon_A < -0.1$ eV). This discrepancy can be explained by the small contribution to the measured Auger electron yield from the Auger transition $L_2 - M_{2,3}M_{2,3}(^1S_0)$. This Auger line is centered at the energy 203.33 eV that is 0.14 eV below the main considered line and has much smaller intensity compared the measured $L_3 - M_{2,3}M_{2,3}(^1D_2)$ Auger line [41].

The effective width model gives results which are quite close to the present calculations as it has been mentioned in Section IIC. Previously the effective width model was used in the Ref. [33] to describe the PCI energy shift of Auger electron emission in the same SRAD process (1) in Ar and demonstrated a rather good agreement with experimental observations. Our calculation within the exact SRAD theory confirms these findings.

Here it is worth to compare the general behaviour of the photoelectron line shapes and the Auger electron line shapes. A comparison of the Figs.4,5 shows the following features.

(i) Line shapes of the photoelectron and the Auger electron are not mirror reflected as it has a place in the SA decay case;

(ii) The PCI distorted photoelectron line shapes have the FWHM of order 0.9-1.1 eV whereas the FWHM of the Auger electron lines are approximately three times smaller, 0.3-0.4 eV.

(iii) The Auger electron line shapes have noticeable asymmetrical shape with slowly decreasing right wing that is usual for the PCI distortion; contrary to this the photoelectron line shapes have more symmetrical form even at small excess energies.

The feature (ii) originates from the large difference of the decay width of the $1s^{-1}$ vacancy state resulting from photoelectron emission and of the $2p^{-1}$ vacancy state which decay yields the Auger electrons. The features (i) and (iii) reflects the fact that the emitted photons participate essentially to the PCI energy exchange.

V. CONCLUSION

The SRAD process following inner atomic shell photoionization has been studied both theoretically and experimentally. We have developed, within the quantum many-body approach, the *ab initio* theory of the PCI effects in the SRAD processes. The general amplitude of the SRAD ionization has been evaluated within semiclassical approximation. Our theory takes into account the interaction between four particles in the final state of the process

considered, namely photoelectron, Auger electron, emitted photon and doubly charged receded ion. The developed theory allows us to calculate and analyze the single and double differential cross section describing the energy distributions of the emitted electrons. These distributions demonstrate the remarkable PCI distortion which proofs to be strongly differ from the case of the single Auger decay of inner vacancy as well as from the predictions of the effective width model developed earlier. The observed new features in the ionization spectra originate from the energy sharing between the three emitted particles: photoelectron, Auger electron and photon.

On the experimental side we have measured the slow 1s photoelectron spectra in Argon in coincidence with the $L_{2,3} - M_{2,3}M_{2,3}$ Auger electrons and the doubly charged receded Ar^{2+} ion following the near threshold 1s photoionization. Such coincidence measurements have allowed us to select reliably the events associated with the SRAD process, revealed the PCI influence on the emitted photoelectrons and confirmed fairly our theoretical findings.

In the considered SRAD ionization of Ar atom the decay width of primary $1s^{-1}$ and intermediate $2p^{-1}$ vacancy states strongly differ, $\Gamma_{1s}/\Gamma_{2p} \simeq 6$. This fact leads to quite different energy spectra of the emitted photoelectrons and the Auger electrons. While photoelectron spectrum has wide energy distribution with FWHM compared with inner vacancy width Γ_{1s}, Auger electron spectrum is much narrow with FWHM close to Γ_{2p}. The PCI energy shift of the photoelectron line is also larger than for the Auger electron line. These features follow from the developed theory and are confirmed by the present measurements of the photoelectron spectra and by the Auger electron spectra measured earlier.

The PCI distortion of the photon emission spectrum strongly depends on the experimental conditions. The PCI effect in the photon spectrum can be observed if it would be measured in coincidence with one emitted electron with fixed energy.

A comparison of our theory with the effective width model shows also the limited character of the latter. It rather well describes the narrow Auger electron spectrum but failed to reproduce the wide photoelectron spectrum. Hence an application of the developed SRAD theory would be very useful for an analysis of the emitted electron spectra in heavy atoms where the important role of the radiative decay of K-shell vacancy increases rapidly with

the atomic number Z.

---

[1] M. Yu. Kuchiev and S. A. Sheinerman, Sov. Phys.- Usp. **32**, 569 (1989).

[2] V. Schmidt, Rep. Prog. Phys. **55**, 1483 (1992).

[3] R. Guillemin, S. Sheinerman, R. Püttner, T. Marchenko, G. Goldsztejn, L. Journel, R. K. Kushawaha, D. Céolin, M. N. Piancastelli, and M. Simon, Phys. Rev. A **92**, 012503 (2015).

[4] R. B. Barker and H. W. Berry, Phys. Rev. **151**, 14 (1966).

[5] F. H. Read, Radiat.Res. **64**, 23 (1975).

[6] G. C. King, F. H. Read, R. C. Bradford, J. Phys. B **8** 2210(1975).

[7] A. Niehaus, J. Phys. B **10**, 1845 (1976).

[8] K. Helenelund, S. Hedman, L. Asplund, U. Gelius and K. Siegbahn, Phys. Scripta. **27**, 245 (1983).

[9] V. N. Ostrovskii, Sov.Phys.-JETP **45**, 1092 (1977).

[10] M. Ya. Amus'ya, M. Yu. Kuchiev, S. A. Sheinerman, Sov.Phys.-JETP **47**, 238 (1979).

[11] M. Yu. Kuchiev and S. A. Sheinerman, J.Phys. B **18**, L551 (1985).

[12] J. Tulkki, G. B. Armen, T. Åberg, B. Crasemann, and M. H. Chen, Z.Physik D, **5**, 241(1987).

[13] G. B. Armen, J. Tulkki, T. Aberg, and B. Crasemann, Phys. Rev. A **36**, 5606 (1987).

[14] G. N. Ogurtsov, J. Phys. B **16**, L745 (1983).

[15] J. Mizuno, T. Ishihara and T. Watanabe, J. Phys. B **18**, 1241 (1985).

[16] A. Russek and W. Mehlhorn, J.Phys. B **19**, 911 (1986).

[17] M.. Yu. Kuchiev and S. A. Sheinerman, Sov.Phys.JETP **63**,1680(1986).

[18] F. Koike, J. Phys. B: At. Mol. Phys.**20**, 1965 (1987).

[19] M. Yu. Kuchiev and S. A. Sheinerman, J.Phys.B **21**,2027 (1988).

[20] F. Koike, J.Phys.Soc.Japan **57**, 2705 (1988).

[21] P. van der Straten, R. Morgenstern, and A. Niehaus, Z.Phys. D **8**,35 (1988).

[22] A. K. Kazansky and N. M. Kabachnik, Phys.Rev. A **72**, 052714 (2005).

[23] S. Sheinerman, P. Lablanquie, F. Penent, Y. Hikosaka, T. Kaneyasu, E. Shigemasa and K. Ito, J. Phys. B: At. Mol. Opt. Phys. **43**, 115001 (2010).

[24] H. Kjeldsen, T. D. Thomas, P. Lablanquie, M. Lavollée, J. H. D. Eland, F. Penent, M. Hochlaf,

and R. I. Hall, J. Phys. B: At. Mol. Opt. Phys. **29**, 1689 (1996).

[25] T. Hayaishi, E. Murakami, Y. Morioka, E. Shigemasa, A. Yagishita, and F. Koike, J. Phys. B: At. Mol. Opt. Phys. **27**, L115 (1994).

[26] F. Koike, Phys. Lett. **193A**, 173 (1994).

[27] S. A. Sheinerman, J. Phys. B: At. Mol. Opt. Phys. **27**, L571 (1994).

[28] S. A. Sheinerman, J. Phys. B: At. Mol. Opt. Phys. **31**, L361 (1998).

[29] L. Gerchikov and S. Sheinerman, Phys. Rev. A **84**, 022503 (2011).

[30] P. Lablanquie, S. Sheinerman, F. Penent, R. I. Hall, M. Ahmad, Y. Hikosaka and K. Ito, Phys. Rev. Lett. **87**, 053001 (2001).

[31] S. Sheinerman, P. Linusson, J. H. D. Eland, L. Hedin, E. Andersson, J.-E. Rubensson, L. Karlsson, and R. Feifel, Phys. Rev. A **86**, 022515 (2012).

[32] R. Guillemin, S. Sheinerman, C. Bomme, L. Journel, T. Marin, T. Marchenko, R. K. Kushawaha, N. Trcera, M. N. Piancastelli, and M. Simon, Phys. Rev. Lett. **109**, 013001 (2012).

[33] S. Kosugi, R. Guillemin, O. Travnikova, T. Marchenko, D. Koulentianos, J.B. Martins et al, Phys. Rev. A **106**, 033114 (2022).

[34] S. Kosugi, F. Koike, M. Iizawa, M. Oura, T. Gejo, K. Tamasaku, J. R. Harries, R. Guillemin, M. N. Piancastelli, M. Simon, and Y. Azuma, Phys. Rev. Lett. **124**, 183001 (2020).

[35] S. Li, D. Koulentianos, S. H. Southworth, G. Doumy, L. Young, D. A. Walko, R. Püttner, J. D. Bozek, D. Céolin, A. Verma, R. Guillemin, M. N. Piancastelli, M. Simon, L. G. Gerchikov, and S. A. Sheinerman, Phys. Rev. A **106**, 023110 (2022).

[36] U. Alkemper, J. Doppelfeld, and F. von Busch, Phys.Rev. A **56**, 2741 (1997).

[37] R. Guillemin, K. Jänkälä, B. Cunha de Miranda et al, Phys. Rev. A **97**, 013418 (2018).

[38] L. O. Werme, T. Bergmark and K. Siegbahn, Phys.Scr. **8** 149 (1973).

[39] M. O. Krause, J. Phys. Chem. Ref. Data **8**, 307 (1979).

[40] M. Jurvansuu, A. Kivimäki, and S. Aksela, Phys. Rev. A **64**, 012502 (2001).

[41] B. Lohmann, X.-K. Meng, and M. Keane, J. Phys. B **25**, 5223 (1992).

[42] J.-P. Rueff, J. M. Ablett, D. Céolin, D. Prieur, T. Moreno, V. Balédent, B. Lassalle-Kaiser, J. E. Rault, M. Simon, and A. Shukla J. Synchrotron Rad. **22**, 175 (2015).

[43] K. Ito, F. Penent, Y. Hikosaka, E. Shigemasa, I. H. Suzuki, J. H. Eland, and P. Lablanquie, Rev. Sci. Instrum. **80**, 123101 (2009).

[44] J. H. D. Eland, O. Vieuxmaire, T. Kinugawa, P. Lablanquie, R. Hall, and F. Penent, Phys. Rev. Lett. **90**, 053003 (2003).

[45] K. Jänkälä, P. Lablanquie, L. Andric, M. A. Khalal, J. Palaudoux, F. Penent et al, Phys. Rev. A **101**, 023413 (2020).

[46] I. Ismail, M. A. Khalal, M. Huttula, K. Jänkälä, J.-M. Bizau, D. Cubaynes et al, Phys. Chem. Chem. Phys. **24**, 20219 (2022).

[47] M. Breinig, Mau Hsiung Chen, G.E. Ice, F. Parente, B. Crasemann, and G.S. Brown, Phys. Rev. A **22**, 520 (1980).

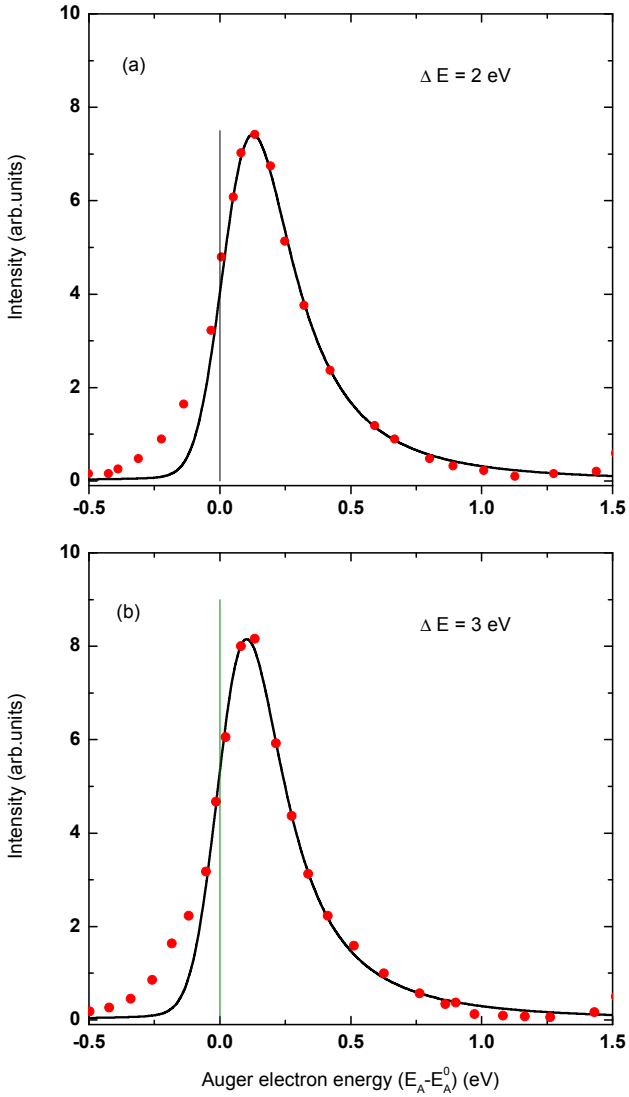

FIG. 5: $L_3 - M_{2,3}M_{2,3}(^1D_2)$ Auger electron energy spectra after the Ar 1s photoionization followed by SRAD process for the excess photon energies 2 and 3 eV (panels (a) and (b), correspondingly). Red circles present the measured values [33] whereas the solid black lines show the calculated curves.